Open Research Online

The Open University's repository of research publications
and other research outputs

Development of a globally optimised model of the cerebral arteries

Journal Item

How to cite:

Keelan, Jonathan; Chung, Emma and Hague, James (2019). Development of a globally optimised model of the cerebral arteries. Physics in Medicine and Biology, 64(12), article no. 125021.

For guidance on citations see FAQs.

© 2019 Institute of Physics and Engineering in Medicine

https://creativecommons.org/licenses/by-nc-nd/4.0/

Version: Accepted Manuscript

Link(s) to article on publisher's website:
http://dx.doi.org/doi:10.1088/1361-6560/ab2479

Copyright and Moral Rights for the articles on this site are retained by the individual authors and/or other copyright owners. For more information on Open Research Online's data policy on reuse of materials please consult the policies page.

oro.open.ac.uk

Development of a globally optimised model of the cerebral arteries

Jonathan Keelan[1], Emma M. L. Chung[2,3] and James P. Hague[1]

[1]School of Physical Sciences, The Open University, MK7 6AA, UK
[2]Cerebral Haemodynamics in Ageing and Stroke Medicine (CHiASM) group, Department of Cardiovascular Sciences, University of Leicester, LE1 7RH, UK
[3]Medical Physics, University Hospitals of Leicester NHS Trust, Leicester Royal Infirmary, LE1 5WW, UK

E-mail: `Jim.Hague@open.ac.uk`

Abstract. The cerebral arteries are difficult to reproduce from first principles, featuring interwoven territories, and intricate layers of grey and white matter with differing metabolic demand. The aim of this study was to identify the ideal configuration of arteries required to sustain an entire brain hemisphere based on minimisation of the energy required to supply the tissue. The 3D distribution of grey and white matter within a healthy human brain was first segmented from Magnetic Resonance Images. A novel simulated annealing algorithm was then applied to determine the optimal configuration of arteries required to supply brain tissue. The model was validated through comparison of this ideal, entirely optimised, brain vasculature with the structure and properties of real arteries. This analysis established that the human cerebral vasculature is highly optimised; closely resembling the most energy efficient arrangement of vessels. In addition to local adherence to fluid dynamics optimisation principles, the optimised vasculature reproduced expected brain perfusion territories, featuring well-defined boundaries between anterior, middle and posterior regions. This validated brain vascular model and algorithm can be used for patient-specific modelling of stroke and cerebral haemodynamics, identification of sub-optimal conditions associated with vascular disease, and optimising vascular structures for tissue engineering applications and artificial organ design.

Keywords: Cerebral vasculature, Computer simulation, Cardiovascular Systems, Mathematical Models, Optimisation, MRI.

1. Introduction

The brain has an exceptionally high demand for oxygenated blood, which accounts for 14-20% of cardiac output, despite contributing only 2% of body mass [1]. This reflects the exceptionally high energy requirements of the brain's active grey matter cells, contained in a thin 2-4 mm layer of cerebral cortex covering the brain's surface. The brain's requirement for an uninterrupted supply of blood has resulted in a highly specialised network of arteries. Major arteries supplying the brain emerge from the Circle of Willis (CoW), a ring-like arrangement of arteries positioned at the base of the brain. The major cerebral arteries (Anterior, Middle, and Posterior Cerebral Arteries - ACA, MCA and PCA, respectively) then penetrate the functional part of the tissue (the brain parenchyma) and branch further to supply the anterior, middle and posterior perfusion territories. These arteries emerge at the surface (pia) of the brain to supply the cerebral cortex (see e.g. Payne[1]). The cerebral cortex features deep folds (gyri) across its surface, upon which the pial arteries attach via perforating arteries that perfuse the grey matter beneath[2]. As the vascular tree branches further into arterioles and capillaries, the tissue environment becomes more symmetric and homogeneous. The area of the vascular bed also increases dramatically, which slows the blood to allow diffusion of oxygen and capillary exchange. Since oxygen diffuses slowly but is metabolised rapidly, the majority of brain tissue lies within 25 microns of a capillary resulting in shorter, more numerous, vessels than seen in other organs [1].

Developing an optimised model of the brain circulation therefore presents a number of technical challenges. Firstly, the brain is supplied by a huge number of vessels with diameters varying across several orders of magnitude. Secondly, the brain posesses a complicated geometry with multiple perfusion territories. Finally, the grey and white matter have differing energy requirements. To identify the most efficient 'idealised' arterial structure capable of supplying an entire brain hemisphere, a simulated annealing (SA) algorithm is implemented for model optimisation. The assumption that configurations of vessels in the adult brain have evolved to be near optimal has not yet been validated through comparison of an ideal (globally optimally efficient) arterial tree with real measurements. This methodological milestone is one of the main aims of this study.

To determine the most efficient arrangement of arteries, it is necessary to identify an algorithm capable of minimising the energy required to supply blood to the tissue, whilst respecting the functionality of the organ. Murray[3] showed that the sizes of parent and daughter vessels in single optimal bifurcations would follow the relation $r_p^\gamma = r_{d1}^\gamma + r_{d2}^\gamma$, where γ is a bifurcation exponent describing the relationship between parent and daughter vessel radii; r the radius of the vessel and subscript p and d represent parent and daughter vessels, respectively. Detailed topological examination of individual bifurcations in, e.g. the cerebral vasculature, supports this relation[4]. Deviations from the optimal conditions predicted by Murray's law have been shown to be associated with vascular disease [5]. Several algorithms have been developed to find vasculatures

consistent with locally optimised bifurcations [6] or fixed bifurcation structures [7]. To computationally obtain globally optimised configurations of arteries, the authors recently proposed a novel Simulated AnneaLing Vascular Optimisation algorithm (SALVO) [8]. Advantages of this algorithm include confident identification of the most fluid-dynamically efficient 'ideal' tree, allowing for implementation of anatomical and physiological constraints, including simulation of hollow organs and penalties for penetrating tissue structures; while treating all length scales using identical optimisation principles. The algorithm was initially applied to modelling the coronary vasculature, through optimising an extensive (>6000 branch) arterial tree for a challenging hollow organ (the heart)[8]. The resulting idealised coronary artery structure was a close match to porcine cardiac morphological data.

Modelling the vascular structure of the brain presents new challenges. Unlike the heart, which can be modelled as comprising of only myocardial tissue, the brain is composed of grey and white matter with very different metabolic demand. These two tissue types have differing volumetric blood flow requirements per mass of tissue[9], which must be factored into the arterial tree generation algorithm. To the best of our knowledge, algorithms for arterial growth capable of global optimisation have not been applied to the vasculature of the brain.

Here, the first globally optimised computational model of the cerebral arteries is presented, developed by minimising the energy required to maintain blood flow. The most efficient configuration of vessels is identified and compared with data from human subjects to explore the extent to which naturally occurring cerebral arterial trees reflect principles of fluid dynamical optimisation. The ability to design efficient arterial trees has potential applications in surgical planning, computational modelling of cerebral haemodynamics, early identification of vascular disease, improved image segmentation from MR and CT angiography, and the design of an optimised vasculature to supply artificial tissues or organs.

In this paper the SALVO algorithm is applied to the cerebral vasculature. The paper is organised as follows. In section 2 the algorithm is described, and details of the segmentation of brain MRI data into grey and white matter are provided. In section 3, the resulting arterial trees are presented and subjected to comparisons with existing morphological *in vivo* data[10, 11]. A summary and outlook are presented in section 4.

2. Materials and methods

In this section, the algorithm used to grow cerebral arterial trees *in-silico* is detailed. The algorithm is similar to the approach for growing cardiac vasculature[8], with some differences for using MRI data to provide tissue information, and some subtleties relating to the supply of cerebral tissue. More detail is included than in Ref. [8].

2.1. Cost Function

At the core of the algorithm is a cost function which measures the fitness of a given tree. It is the sum of (a) the metabolic cost to maintain blood (b) the cost for pumping blood (c) a requirement to supply blood evenly to all tissue and (d) a penalty for large vessels that cross parenchyma, which can be written as:

$$C_{\mathrm{T}} = A_{w,v}(C_w + C_v) + A_o C_o + A_s C_s \tag{1}$$

where $A_{w,v}, A_o$ and A_s are dimensionless constants that scale each contribution to the cost function. C_v is a metabolic cost for maintaining blood volume and C_w is the cost of pumping through a vessel. In addition, C_s is a penalty for over- or under-supplying tissue and C_o is a penalty associated with vessels that penetrate tissue. To form physiological trees, A_s, has a large value since tissue without supply would die. A high (but slightly lower) value of A_o heavily penalises vessels that cut through parenchyma to affect organ function. Therefore A_s and A_o act as constraints.

2.1.1. Pumping cost Following Murray[3], Poiseuille flow is assumed to calculate the power dissipated during flow through a vessel, W_i,

$$W_i = \frac{8\mu l_i f_i^2}{\pi r_i^4} \tag{2}$$

where f is volumetric flow rate, vessels are cylindrical with radius r and length l and a representative value is used for the viscosity of blood $\mu = 3.6 \times 10^{-3}$Pa s (although it is noted that blood viscosity can drop significantly in small vessels $< 100\mu$m[12]). The total power dissipation, $C_w = \sum_i W_i$ is calculated by summing over all vessels, i.

For computational efficiency, a constant input flow is maintained, and terminal flows are fixed and equal. Thus, from conservation of mass, the flow in any artery depends only on the number of terminal sites downstream. If f_{root} represents total flow into the tree, the total flow per end node is $f_{\mathrm{term}} = f_{\mathrm{root}}/N_{\mathrm{end}}$. A power law is used to relate radii and flow[13], $f = \epsilon r^{\gamma}$, where γ is the bifurcation exponent which is set from experimental considerations and ϵ is a constant determined from f_{root} and r_{root}.

2.1.2. Metabolic cost for maintenance of blood volume Following Murray[3], a metabolic cost to maintain a volume of blood is assumed:

$$C_v = m_b \sum_i V_i. \tag{3}$$

The value $m_b = 648$J s^{-1} m^{-3} is chosen, which is within the measured range for humans[14]. V_i is the total volume of a cylindrical arterial segment.

2.1.3. Blood Supply Penalty In a healthy organism, perfusion is uniform throughout tissue over a physiologically long timescale[15]. Thus, terminal nodes need positioning so that the supply is uniform. The terminal nodes in SALVO are much larger than capillaries, so terminal nodes are considered to be surrounded by spherical

microcirculatory "black boxes"[6] of radius R_{supply}. Within each sphere the details of the microvasculature are neglected. Without this assumption the computational power required to optimise the tree would be prohibitive. The radius of the spheres is calculated using physiological values for the blood demand of the tissue as,

$$4\pi R_{\text{supply}}^3/3 = f_{\text{term}}/q_{\text{req}}, \tag{4}$$

where q_{req} is the volumetric blood flow required to maintain tissue. Grey and white matter in the brain have different supply requirements[9], $q_{\text{req,grey}} = 10.9 \times 10^{-3}$ $(\text{m}^3/\text{s})/\text{m}^3$ and $q_{\text{req,white}} = 3.57 \times 10^{-3}$ $(\text{m}^3/\text{s})/\text{m}^3$ respectively (see table 2), leading to a smaller R_{supply} and thus higher density of terminal nodes sited in the grey matter. The total flow is determined using q_{req} and the total volume of grey and white matter in the MRI scans, which are 389.12×10^{-6} m^3 and 321.64×10^{-6} m^3 respectively (see Sec. 2.2).

There is no unique way to define the supply penalty. For this paper,

$$C_s = \sum_{\textbf{voxels}} s;\ s = \begin{cases} 10 & \text{if } b = 0 \\ (b-1)^2 & \text{otherwise} \end{cases} \tag{5}$$

where b is the total number of spheres contributing to the supply of a single tissue voxel. Voxels representing the spatial locations of tissue are identified from MRI imaging and the sum is performed over all tissue voxels. The collection of voxel data is described later in Sec. 2.2. C_s favours voxels supplied by a single sphere, and thus encourages dense packing of supply spheres while minimising overlap. This cost only needs to be recalculated when terminal nodes move.

2.1.4. Exclusion of Large Arteries Larger arteries are absent from regions of many organs as they would interfere with function. For example the brain has pial arteries running across its surface, whereas only the smaller branches from these arteries are allowed to penetrate. Also, the higher blood supply requirements of grey matter[9] may play a role in bringing larger arteries to the surface.

A distance map is used to calculate a penalty that increases with vessel depth within the excluded tissue, thus enforcing exclusion of larger vessels. A cutoff radius R_{ex} is defined whereby any node exceeding this radius incurs a cost,

$$C_o = \sum_{R > R_{\text{ex}}} D_{ijk \in S}^6, \tag{6}$$

where i, j and k are voxel coordinates, S is the line segment corresponding to the vessel and D_{ijk} is the distance map value, which is calculated from MRI data as discussed in the next section [8].

Cerebral arterioles with diameters less than $\sim$ $100\mu m$ are responsible for penetrating deep within cortical tissue[2]. For even the largest trees considered here the smallest vessels are slightly wider than this value. $R_{\text{ex}} = 150\mu\text{m}$ is selected to ensure some penetration into the tissue, and to understand how results are modified by changes in R_{ex}.

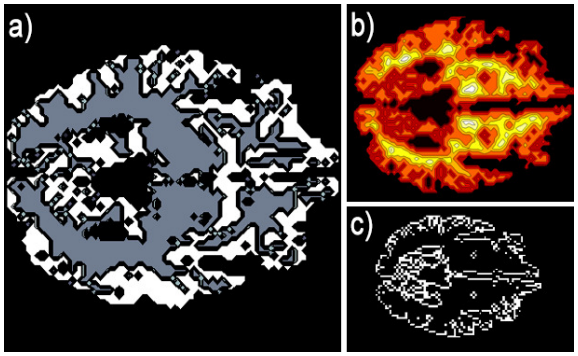

Figure 1. An image slice of the MRI data from a healthy individual, at various stages of analysis. Panel a) shows the segmented tissue, b) shows the result of the distance map calculation, c) shows the identified surface voxels.

2.2. Tissue voxel map and MRI data

In a modification to the previous algorithm[8], MRI data are used to provide realistic tissue shapes. A T_1-weighted image from a healthy individual (one of the authors) was acquired using a 3T Siemens Skyra MR scanner (Siemens Medical, Erlangen, Germany). Spatial resolution for the image was $0.75 \times 0.75 \times 0.8$ mm^3. Images were exported for processing in DICOM format. A time-of-flight (TOF) angiogram was also taken to locate the root positions of the MCA, ACA and PCA. The T_1-weighted image was segmented into white and grey matter using the statistical parametric mapping function in MATLAB (MathWorks, Natick, MA, USA) [16]. Before calculation, MRI images were downscaled using the MATLAB function *reducevolume* by a scale factor of 3 to a resolution of $2.25 \times 2.25 \times 2.4$ mm^3 to reduce computational time. Surfaces of the combined white and grey matter were identified via a nearest neighbour search, where voxels having at least one unoccupied neighbour were labelled as belonging to the outer surface of the brain. Each voxel in the tissue was assigned a value equal to the shortest distance to the surface (the distance map[17]). A sample slice at each stage of the segmentation process is shown in Fig. 1. Following segmentation, the brain was divided into left and right hemispheres and SALVO was performed for a single hemisphere (the left hemisphere). Running the algorithm on a single hemisphere reduces the total number of nodes required, reducing the overall simulation time, and is justified since vessels downstream of the Circle of Willis do not typically cross between hemispheres.

Since MCA, PCA and ACA inputs are very closely spaced, a single arterial inlet is provided to the SALVO algorithm, representing the approximate position of these arteries as they branch from the CoW. Relative flows are then calculated by the optimisation algorithm. Currently it is not possible to predict the structure of anastamoses such as the CoW.

2.3. Simulated Annealing (SA)

There are a variety of options available for optimising the cost function to obtain a vascular network. Simulated Annealing (SA), which is a general optimisation technique inspired by the physical process of annealing[18], was selected as it provides both simplicity of implementation and certain guarantees regarding convergence to the global minimum. In SA, sequential random updates are made to a trial solution, and the probability of accepting each update is given by the Metropolis scheme,

$$P_{ij} = \min\left\{\exp(\frac{-\Delta C_{ij}}{T}), 1\right\} \tag{7}$$

where P_{ij} and $\Delta C_{ij} = C_j - C_i$ are the probability and change in cost associated with altering tree configuration i to configuration j, respectively. T is the annealing temperature, which must be slowly reduced. P_{ij} permits occasional acceptance of modifications that increase the cost, allowing the solution to climb out of local minima. Equation 7 is in some sense problem independent and this part of the algorithm is straightforward to implement; adapting SA to a specific problem involves choosing algorithms to efficiently generate new trial solutions. Over the following sections we describe the update procedure and specific implementation in detail.

The annealing temperature must be reduced suffiently slowly to explore the configuration space thoroughly. The initial temperature, T_{init}, was chosen to be much higher than the cost change associated with a typical update, so that initially almost all modifications to the tree are accepted. T_{final} is set such that at the end of the SA algorithm, only changes that reduce the overall cost are accepted. To proceed from T_{init} to T_{final}, the following temperature schedule was used,

$$T_{n+1} = \alpha T_n \tag{8}$$

where n denotes the SA step and

$$\alpha = e^{\frac{1}{S}(\ln T_{\text{init}} - \ln T_{\text{final}})}, \tag{9}$$

where S is the total number of SA steps. This exponential schedule is common in simulated annealing algorithms.

2.4. Arterial tree updates

In the SALVO algorithm, the arterial tree is represented as a binary tree. This is consistent with the observation that (ignoring the capillary mesh) $\sim 94\%$ of branchings in the cerebral vasculature are bifurcations [2]. Arteries in the model vasculature begin at the level of the major cerebral arteries (radii $\sim$1.5 mm) and the tree branches at bifurcation nodes until reaching arterioles of size $\sim 100\mu$m. The root node represents the end of the largest artery, and bifurcations occur at each node. The tree terminates with a total of N_{end} terminal nodes, and as the radii of arteries decrease at each bifurcation these nodes represent the smallest vessels modelled. Each bifurcation and terminal node of the tree has a 3D coordinate. Bifurcations are connected via straight vessels.

At each SA step, either of the following updates are made: (1) move a node, or, (2) swap node connections to change the tree topology. This minimal set of updates guarantees ergodicity (i.e. the algorithm can explore any tree configuration). 80% of updates are selected to be type (1) and 20% type (2).

The steps for update of type (1) are:

(i) Select a node type and update distance at random according to the weightings in the first four rows of Table 1.

(ii) Randomly choose a node from either the set of terminal or set of bifurcating nodes from the tree according to the corresponding node type in the table.

(iii) For each spatial dimension generate a node displacement using a uniform random number between $-d_{\text{move}}$ and d_{move}, where d_{move} is the maximum displacement distance, which is either short distance ($d_{\text{move}} = 1$mm) or long distance ($d_{\text{move}} = 10$mm) according to the update distance in the table.

(iv) Add the displacement to the position of the randomly chosen bifurcation.

(v) Calculate cost change and accept or reject according to the Metropolis condition.

The move update is summarised in figure 2(a). The reason for selecting terminal and bifurcating nodes separately is to speed up the algorithm: the need to recalculate the supply cost for terminal nodes means that moves of those nodes cost significantly more computational time than moves of bifurcating nodes. The reason for selecting moves of short and long ranges is a compromise to keep acceptance rates as high as possible: long range moves help the algorithm at high anneal temperatures and short range moves lead to higher acceptance rates at low temperatures.

Steps for update (2) are:

(i) Randomly choose two nodes from the set of all nodes.

(ii) Check if either node is upstream of the other.

(iii) If either node is upstream of the other, repeat steps 1 and 2 until a valid pair is found

(iv) Swap the parent indices of the nodes.

(v) Calculate cost change and accept or reject according to the Metropolis condition.

The swap update is summarised in figure 2(b). Update weightings are summarised in table 1. The root node is never updated.

We note that the swap node update simply swaps the parent indices of the two nodes without making any moves. The cost of making this kind of simple index swap is small, with subsequent move updates ensuring ergodicity. This occasionally leads to trial configurations where vessels span the whole hemisphere. Such states are valid trial configurations and are essential for ergodicity in the algorithm (i.e. that all possible states can be examined, even if they are very unlikely and rejected at low temperatures).

Table 1. Weightings, parameters, and target nodes for updates in the SA algorithm. Update are selected according to the probability weight shown.

Type	Parameter	Target	Weight
Move	$d_{\text{move}} = 1\text{mm}$	bifurcation	0.675
	$d_{\text{move}} = 1\text{cm}$	bifurcation	0.075
	$d_{\text{move}} = 1\text{mm}$	terminal node	0.045
	$d_{\text{move}} = 1\text{cm}$	terminal node	0.005
Swap	none	any node	0.2

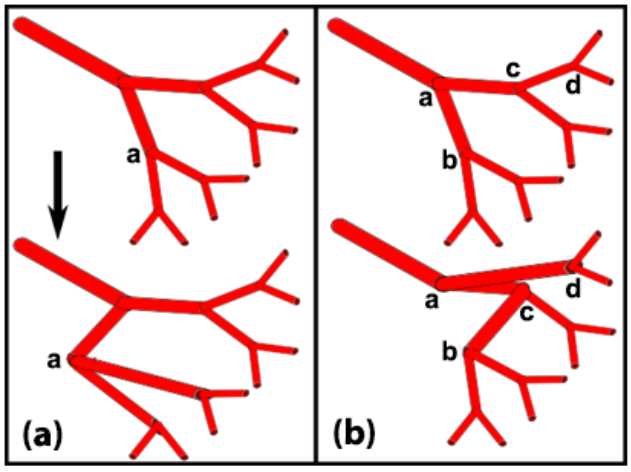

Figure 2. A summary of updates. In panel (a) node a is moved. In panel (b) parents of two nodes (nodes b and d) are swapped. The parent of node b is node a, and the parent of node d is node c. After the swap, the parent of node b is node c and the parent of node d is node a (reproduced from Ref. [8]).

Other update options are possible. For example, an alternative would be to maintain the relative positions of the downstream vessels during the swap. The cost of making moves to the whole downstream tree at the same time would be huge (the worst case being a swap of the daughters of the root node, where calculating the difference to the cost function would involve recomputing the whole function), and most of the swaps carried out in that way would be rejected because they would lead to a lack of supply to regions of the tissue. The updates used here are the simplest, and most efficient ones that we identified that also ensure ergodicity.

2.5. Outline of the algorithm

The whole SALVO algorithm is now summarised. The initialisation steps are as follows:

(i) Generate a maximally asymmetric tree with $N = 2N_{\text{end}} - 1$ terminal nodes by (a)

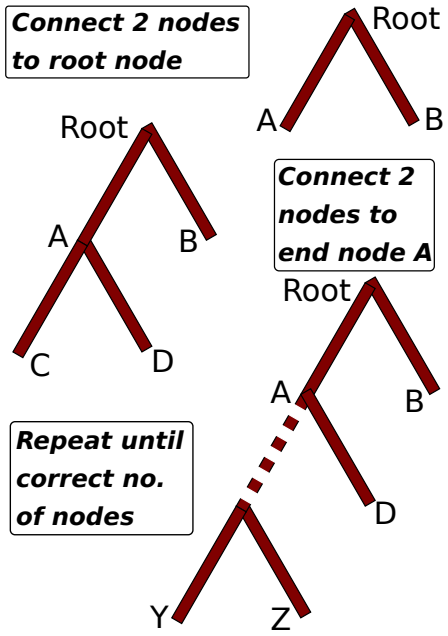

Figure 3. Generation of maximally asymmetric tree during initialisation.

connecting the root node to two terminal nodes (b) attaching two nodes to one of the most recently attached nodes (c) repeating step (b) $N-1$ times. An example of this procedure is shown in figure 3.

(ii) Calculate $f_{\text{term}} = f_{\text{root}}/N_{\text{end}}$

(iii) Assign the position of each non-terminal node of the tree to a random location in space.

(iv) Assign each terminal node a random position inside the tissue area to be perfused.

(v) Randomise the topology of the tree by repeatedly applying the swap node update $1000 \times N$ times.

(vi) Calculate flows through all nodes. An efficient method is: Starting from a terminal node visit parent nodes until the root node is reached. Add f_{term} to the flow variable of each node visited. Repeat for all terminal nodes. Since flow is conserved, at the end of this procedure the flow through the whole tree is known.

(vii) For each node, calculate its radius $(f/\epsilon)^{1/\gamma}$.

(viii) Calculate the initial value of the cost function using Eq. 1.

Once initialised, the tree is in a random but valid topological and spatial state. The optimisation procedure is as follows:

(i) Randomly choose and apply an update using the weightings found in table 1.

(ii) Calculate the cost function (Eq. 1) for the newly modified tree.

(iii) Using Eq. 7, accept or reject the modification. If rejected, revert the tree to its previous state.

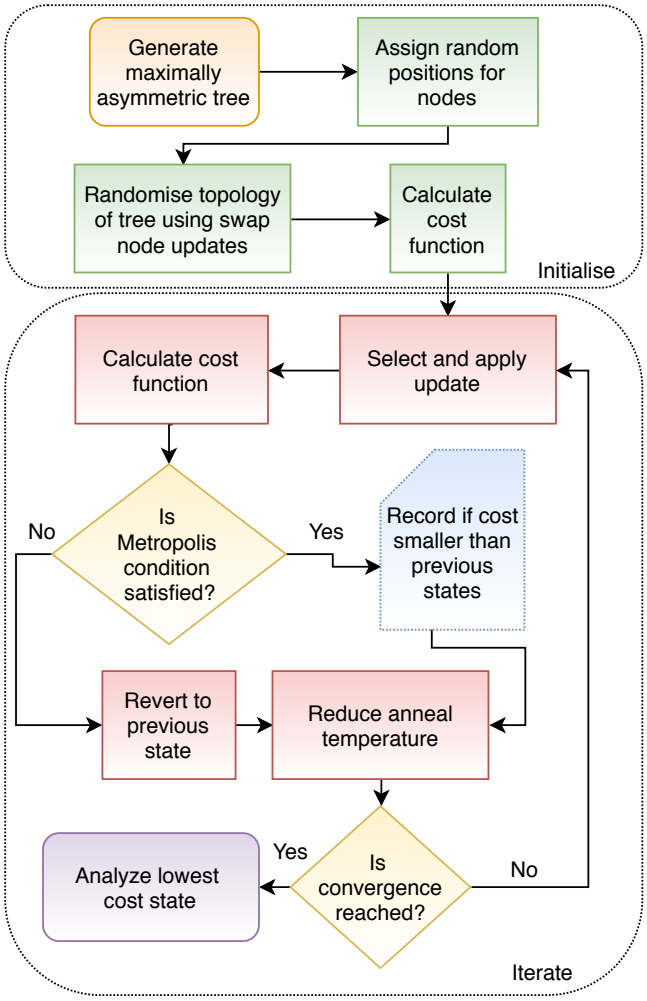

Figure 4. Flowchart showing steps in the algorithm.

(iv) If the cost function of the trial vasculature is smaller than all previous states, then record the tree state.

(v) Reduce the SA temperature following Eq. 8.

(vi) Repeat the previous steps S times.

A flowchart can be found in figure 4. A full list of parameters used in the SALVO algorithm is provided in table 2. We selected an exclusion radius of $R_{\text{ex}} = 150\mu$m, and input radius of 1.5mm throughout. For large trees, the total number of topological states is vast, and good optimisation can only be achieved for very large numbers of SA steps. The program was implemented in C++ making full use of the 2011 standard library, and was compiled with the O3 flag for maximum optimisation. Subsequent data analysis of the generated trees was performed using a mix of Python and C++. The algorithm was not parallelised since simulated annealing is very challenging to parallelise and speedups are often mediocre (see e.g. [19]). The optimisation of an 8191 node tree in a realistic geometry takes several days on a single Intel i7 core. The Open University IMPACT cluster was used to carry out multiple calculations with different random number seed

Table 2. Input parameter names, symbols, values and typical sources.

Parameter	Symbol	Value	Source
Flow requirement (grey)	$q_{\mathrm{rec,grey}}$	10.9×10^{-3} $(\mathrm{m}^3/\mathrm{s})/\mathrm{m}^3$ brain	SPECT [9]
Flow requirement (white)	$q_{\mathrm{rec,white}}$	3.57×10^{-3} $(\mathrm{m}^3/\mathrm{s})/\mathrm{m}^3$ brain	SPECT [9]
Volume (grey)	V_{grey}	389.12×10^{-6} m^3	MRI (Sec. 2.2)
Volume (white)	V_{white}	321.64×10^{-6} m^3	MRI (Sec. 2.2)
Root flow	$q_{\mathrm{rec,grey}}V_{\mathrm{grey}}$		
	$+q_{\mathrm{rec,white}}V_{\mathrm{white}}$	323.4 ml / min	Calculated
Root radius	r_{root}	1.5 mm	Estimated
Root position	N/A	Average of MCA, PCA, ACA	MRI (Sec. 2.2)
Branching exponent	γ	3.2	MRI (Sec. 2.6)
Metabolic constant	m_b	648 J $\mathrm{s}^{-1}\mathrm{m}^{-3}$	From [14]
Node exclusion parameter	R_{ex}	150μm	Estimated [2]
No. end nodes	N_{end}	4096	Selected
SA steps	S	10^{10}	Selected
SA initial temperature	T_{init}	10^{12}	Selected
SA final temperature	T_{final}	10^{-10}	Selected
Cost function weight	$A_{w,v}$	1×10^4	Selected
Exclusion penalty	A_o	1×10^{15}	Selected
Supply penalty	A_s	1×10^{30}	Selected

(RNS) and large tree sizes. Several anneal runs were made, and the tree with the smallest value of the cost function was selected for analysis. The standard deviation of the final cost function over all annealing runs was 0.6% of the minimum cost. The number of tree combinations and thus timescale for optimisation grows rapidly with tree size, and we were far from convergence for an ∼16000 node tree after a 2 week anneal (standard deviation in cost function is still around 30%). We estimate that the algorithm would need to run for at least 10x as long for acceptable optimisation of such a tree.

2.6. Comparison data

Comparison trees were taken from the BraVa database[10, 11]. Wright *et al.* extracted cerebral arterial tree morphometry from 3T time-of-flight MRA high-resolution images, and then segmented the trees manually from MRI image slices using the ImageJ software package. Wright *et al.* classified arterial segments using Strahler ordering, which can lead to groupings of arteries of vastly different diameters. To mitigate this issue, the data were reanalysed to use diameter defined Strahler order (DDSO) to improve the classification of vessel segments[20]. A modified DDSO (MDDSO) procedure was used to account for data that are not Gaussian distributed (see appendix). Trees were discarded from the dataset if they had any arteries labelled as zero radius or if the MDDSO algorithm failed to converge. The majority of trees from human subjects had 5 MDDSOs, and trees with 5 and 6 MDDSOs were analysed separately. The analysis procedure was identical for MRI and computational trees.

The BraVa MRI data exhibit discretization due to the 0.31 mm voxel resolution. In order to obtain a more meaningful comparison of our generated trees to the BraVa data [10, 11] the effects of MRI resolution were replicated in the computational trees. The effect of the MRI and subsequent segmentation was to prune small arteries from the tree and discretise the radius, which was relatively straightforward to replicate in the artificially generated trees by including only arteries with radius greater than a cutoff, R_C, and discretising the radius in steps of R_C above this value by rounding down to the nearest multiple of R_C (this discretisation originates from voxelisation and was seen in the BraVa data). For around 20% of the radii, an additional voxel width was added at random to emulate aliasing effects for vessels that sit close to voxel boundaries and therefore appear to be one voxel wider than their true width. $R_C = 0.228$mm was chosen so that it was as close as possible to the MRI resolution cutoff, while maintaining the same number of Strahler orders as the MRI data. This procedure was repeated 27 times with different random number seeds with means and variances calculated from the resulting set of data.

Sensitivity analysis for 2D trees (to be published separately) indicates that the tree structure is only sensitive to the bifurcation exponent, γ. Bifurcations in the BraVa data were analysed to estimate the bifurcation exponent. Results are shown in Fig. 5, with mean value found to be $\gamma = 3.2$. Therefore, $\gamma = 3.2$ was used for all computational trees.

2.6.1. Analysis We compare the generated and MRI arterial trees both qualitatively and quantitatively. There are two qualitative analyses. Qualitative analyses involve visual comparison of the generated trees to both schematic visualisations of the cerebral arteries in Gray's anatomy (See Figs. 19.2 and 19.4) [21] and to the MRI trees of Wright *et al.*. Qualitative analysis also examines the perfusion territories of the major cerebral arteries. As computational trees begin with only a single root node, any "major" arteries identified in the final trees arise naturally as a result of our optimisation procedure. This

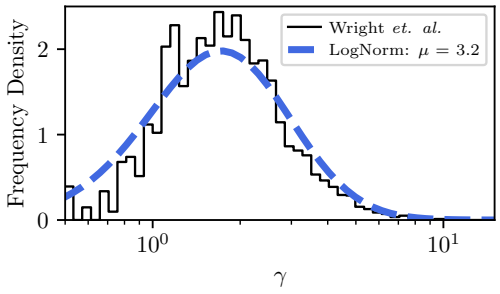

Figure 5. Histogram showing the distribution of γ values in the BraVa data[10, 11]. Fit of a log normal curve to the histogram finds a mean value, μ, of 3.2 for γ.

presents a slight difficulty, as the nodes corresponding to the MCA, PCA and ACA must be identified after the optimisation has occurred. To do this, we select triplets of nodes which are toplogically as close as possible to the root, and whose total set of end nodes contain all end nodes in the tree with no duplication. These constraints limit the number of available triplets considerably, though there are still multiple valid choices. Fortunately this has very little effect on the identified perfusion territories, and so choice in selecting perfusion territories is fairly limited. Once the three "root" nodes have been identified, we create the perfusion territories by colour coding the tissue voxels according to which of the three "root" nodes is attached to the terminal node closest to that voxel.

Quantitative analysis involves comparison of key morphometric and physical characteristics of the MRI and simulated trees. We initially analyse both the computational and MRI derived trees by assigning a Modified Diameter Defined Strahler Order (MDDSO) number to each artery. The arteries of each tree can then be grouped by the MDDSO, and average quantities (including radii, lengths and branching ratios) can be calculated for each group. We examine and compare three quantities in detail: the radii, the lengths and the branching ratios. We define the branching ratios as $r_p/r_{d>}$ and $r_p/r_{d<}$, where r_p is the parent vessel radius, $r_{d>}$ and $r_{d<}$ are the radii of the larger and smaller daughter vessels in the bifurcation respectively. Plotting each of these quantities as a function of MDDSO shows how they vary as a function of the topology of the tree.

3. Results

Figure 6 shows the appearance of the vasculature as viewed from various angles generated for a single hemisphere with $N = 8181$, and symmetrised about the centre of the brain before rendering with POV-ray[22]. Large sections of the arteries run across the outer surface of the brain, mimicking the pial arteries.

Looking from the inferior aspect, the single input quickly divides into 3 large arteries supplying the anterior, lateral and posterior portions of the brain, corresponding to the anterior cerebral artery (ACA), the middle cerebral artery (MCA), and the

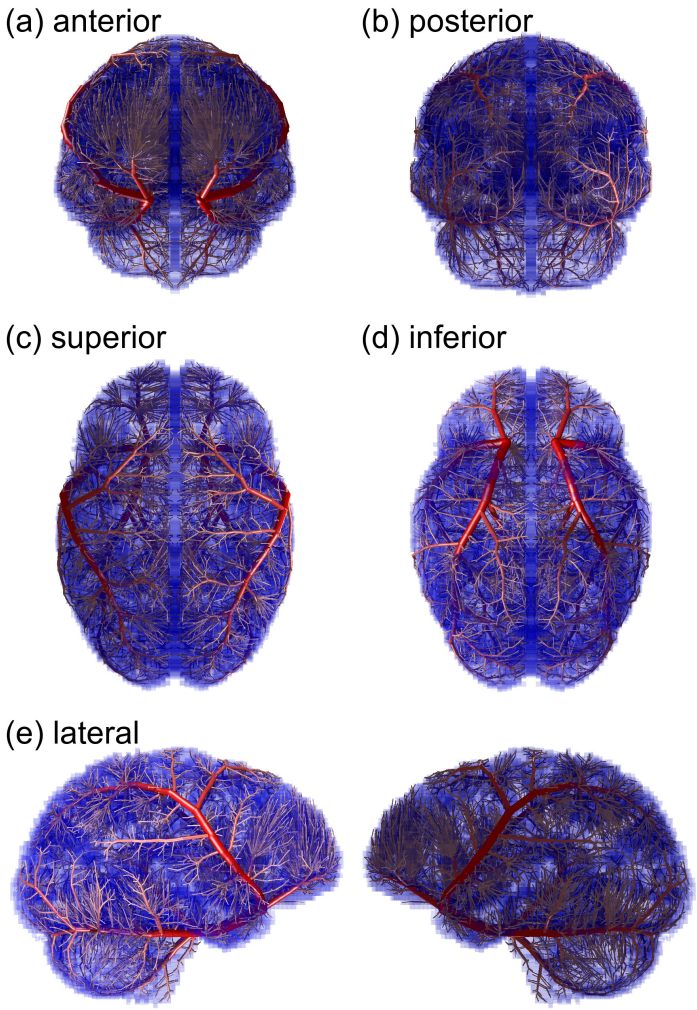

Figure 6. Cerebral vasculature automatically generated for segmented grey and white matter geometry obtained from MRI imaging (8191 seg.). The vasculature is grown on a single hemisphere and then symmetrised. Note, vessel radius has been doubled in the images to improve visibility of the smaller vessels.

posterior cerebral artery (PCA) and cerebellar arteries respectively. Looking from the inferior view, the single input quickly divides into 3 large arteries supplying the anterior, posterior and lateral regions of the brain. The large artery to the front roughly corresponds to the anterior cerebral artery (ACA), that to the side to the middle cerebral artery (MCA) and the large artery directed to the rear the posterior cerebral artery (PCA) and cerebellar arteries. The MCA flows up the fissure of Sylvius. The approximate form is very similar to textbook schematics of the cerebral arteries that can be found in e.g. Ref. [21] (see Figs. 19.2 and 19.4 of that reference). The algorithm presented here only considers branching trees with no mechanism to generate anastamoses, so the Circle of Willis is not reproduced.

To provide a comparison with real vessels, the cerebral vasculature of patient BG001

from the BraVa database is rendered in figure 7. In the figure, the vasculature is superimposed onto the brain shape (in blue) from our MRI scan, which has been scaled to the approximate size of the original tissue to provide a guide to the eye. This is necessary since the BraVa database only contains vessel data, but not brain outlines. The anterior view shows how the MCA passes around the brain in the vicinity of the fissure of Sylvius as in the model. The ACA passes up between the hemispheres in the real vasculature, whereas in the model the ACA is slightly displaced to the sides. Also seen from the inferior view is the circle of Willis (CoW), which can not be reproduced in our model. However six vessels emerge from the CoW in a similar way to those emerging from the root node of our model. In the model the confluence of large vessels representing the CoW is slightly further forward than in the real vasculature. The vessels in the model are generally straighter and less tortuous, as can be seen clearly in the MCA territories in the lateral view.

Figure 8 shows the perfusion territories of the three large vessels emanating from the input vessel, with each colour representing a perfusion territory. Again the single hemisphere has been symmetrised about the mid-saggital plane. Views are shown from a variety of directions. The perfusion territories are well differentiated between the anterior, middle and posterior regions of the brain, consistent with clinical observation [10]. The MCA territory (yellow and blue) occupies most of the superior and lateral regions of the brain. The ACA territory (green and cyan) is found towards the front of the brain. The third territory (purple and red) supplies the posterior regions of the brain and the cerebellum, roughly representing the perfusion territory of the PCA and cerebellar arteries.

Figure 9 shows the mean arterial radius, r, plotted vs MDDSO. MRI data were averaged over all trees, whereas the computational data is averaged over only the tree with lowest cost. Error bars show 25th and 75th percentiles of the data. For the radius, general agreement with MRI data is good. The levelling out of the radius seen in the MRI data for smaller Strahler orders may be related to overestimation of the smallest radii in the MRI data due to resolution effects. The overall behaviour of the radii as a function of branching order is consistent between the MRI and generated data.

Branching ratios are shown in Fig. 10. Branching ratios are expected to tend to $1/2^{1/\gamma}$ (approximately 0.8 for $\gamma = 3.2$) since arterial trees must necessarily become more symmetric as they become smaller. This can be understood by considering the final arterioles before the capillary bed, which are of roughly equal size, so the final bifurcation before the capillary bed must be roughly symmetric.

Finally in Fig. 11 the relationship between length and branching order for the generated tree is examined. Figure 11 shows the mean lengths of the vessels vs MDDSO. For length measurements, the pruning procedure is very important, since the effect of finite MRI resolution is the absence of small branches from major vessels in the MRI data, potentially leading to overestimation of segment length. On the other hand, computational data have only short lengths between bifurcations due to large numbers of small vessels branching from major arteries that would not be imaged by MRI, and thus

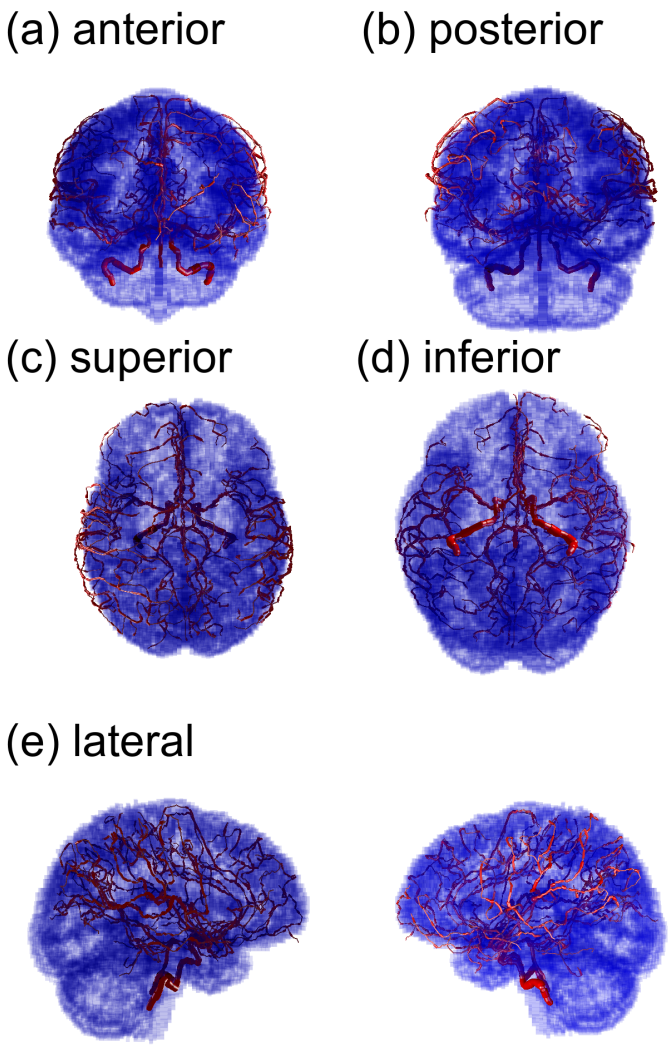

Figure 7. Cerebral vasculature of patient BG001 from the BraVa database. The BraVa database only contains vessels, but not scans of tissue, so the vasculature is superimposed on a brain shape (in blue) from our MRI scan and scaled to fit to provide a guide to the eye.

obscure the comparison. Examining the pruned data, the mean lengths of the largest Strahler order are roughly consistent between measured and *in-silico* trees. Lengths of vessels in the MRI data appear to increase slightly as radius decreases, whereas the pruned computational data has roughly constant length.

4. Discussion

One of the main aims of this study was to provide researchers with an algorithm for simulating arterial trees that overcomes some of the well known limitations of CCO techniques. Our approach to vascular modelling adopts a simulated annealing approach to identify a globally optimised solution. Using the brain as an example, we demonstrate

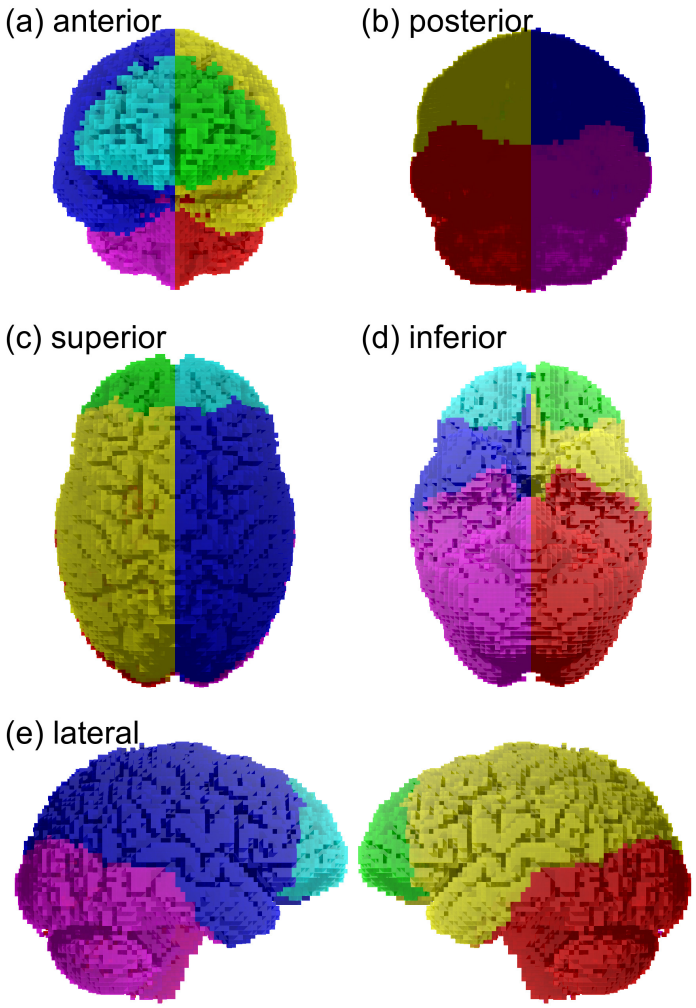

Figure 8. Perfusion territories of the three large generated vessels viewed from various angles. Each territory is denoted with a different colour. The perfusion territories have well defined boundaries between anterior, middle and posterior regions.

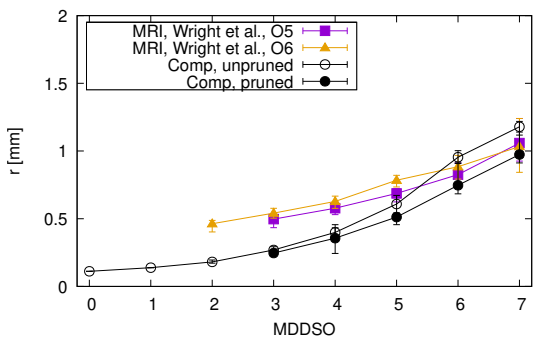

Figure 9. Plot showing the mean radii of the generated tree vs the MRI data of Wright *et al.*[10, 11] as a function of modified diameter defined Strahler order (MDDSO). Bars show 25th and 75th percentiles.

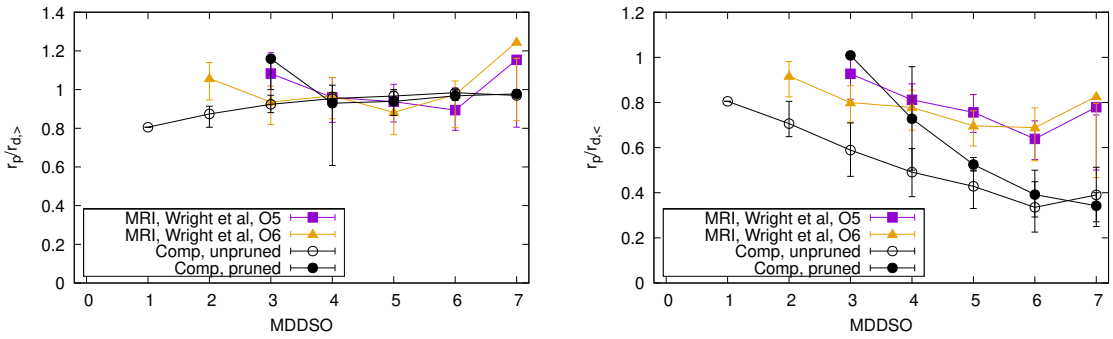

Figure 10. Plot showing the branching ratios, $r_p/r_{d>}$ and $r_p/r_{d<}$, vs MDDSO for MRI and *in-silico* data. Bars show 25th and 75th percentiles.

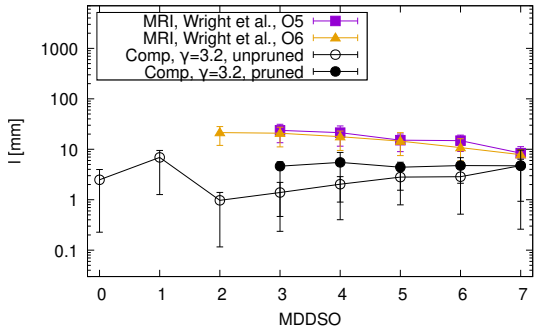

Figure 11. Plot showing the mean lengths of various branches of the generated tree in comparison to MRI BraVa data[10, 11] as a function of branching order. Bars show the 25th and 75th percentiles.

that these methods are easily extended to include complex tissue morphology (obtained from imaging data) and multiple substrates. Advantages of simulated annealing include the ability to apply generalised principles over multiple length scales. Simulations require virtually no adjustment from the user, other than initial starting information regarding the geometry and metabolic demand of the tissue substrates being supplied. This simple approach, using a single starting node per hemisphere, with no angiographic information included in the model, generates arterial trees that are strikingly similar to real arteries. Morphological analysis shows that the radii and branching ratios of vessels in the human brain and optimised trees, have the same overall trends with many points lying within the biological variance, although some points are less well represented. The radii are well matched for large Strahler order, but underestimated for smaller orders. The branching ratios of the largest daughter match well for all orders. The branching ratios of the smaller daughter vessel is underestimated for large Strahler order but there is agreement for smaller orders. The lengths of vessels are systematically shorter than found in MRI data. Agreement in lengths improves significantly once the pruning effects of MRI resolution are taken into account. The structure of our simulated trees was surprisingly similar to images of the human cerebral vasculature, with 'pial arteries' traversing the surface of the brain, MCA traversing the fissure of Sylvius,

and three major artery territories corresponding closely to ACA, MCA and PCA + cerebellar perfusion territories. We conclude that the cerebral arteries have evolved, through physiological principles, to efficiently minimise energy consumption resulting in close morphological similarities between the real brain and a globally optimised 'ideal' configuration of arteries.

There are a lot of strengths to our method. Ours is the first method to find the globally optimal arterial tree structure for the brain with the ability to change the topography of the tree to explore all possible structures. The method can treat grey and white matter metabolic demands separately, ensure that all tissue is supplied, that large vessels respect parenchyma, with a realistic tissue structure derived from MRI. The simulated annealing approach is extensible, so changes to the form of the pumping cost to include more detailed physics are straightforward. Venous drainage could also be included, although this is more challenging and work to do this is in progress. To our knowledge, no other arterial growth method can make such close connection to the major arteries of the cerebral vasculature without direct reproduction from vessels derived from imaging.

As improvements are made to the algorithm, additional applications are expected. Vascularisation of artificial tissue is a major problem that limits the size of the tissue, and thus the ability to grow replacement tissue for transplant. The SALVO algorithm could be used to design top-down vasculatures for artificial tissue and eventually organs. SALVO could be used to fill in gaps in angiography imaging in a similar manner to Linniger *et al.*[23]. Also, the algorithm has immediate applications to any problem that requires knowledge of the flows from the cerebral arteries, such as stroke modelling that could be used to enhance intraoperative monitoring [24].

It is appropriate to put the algorithm presented here into the context of several other schemes for *in-silico* arterial 'growth'. Early approaches use stochastic methods based on morphological data[25]. A number of algorithms attempt to mimic 'sprouting angiogenesis'. This works best when modelling disordered arterial trees associated with malignant tumour growth[26]. Previously developed growth-based algorithms are not yet generalisable to the growth of arterial trees for large organs [27].

A local optimisation technique, Constrained Constructive Optimisation (CCO), has been used extensively to generate large arterial trees [6, 28]. However, local optimisation at individual vessel junctions does not generally result in the most efficient overall tree. CCO also has limitations when applied to hollow organs, and tends to generate trees that are too symmetric (especially for the largest arteries)[29, 30]. This situation can be improved by combining CCO with medical imaging of e.g. the large cerebral arteries, leading to impressive results[23], however, no single algorithm based on CCO can handle all of the required length scales. The CCO derived global constructive optimisation technique makes a global pruning update, and improves on CCO by allowing additional local modifications to the topology of the tree, however the minimisation approach used offers no guarantee of reaching the true global minimum [31].

Kaimovitz *et al.*[7] previously developed a hybrid approach for the myocardium,

making heavy use of morphological data to grow very large trees featuring both arteries and veins. The trees grown are impressively large, but their method is difficult to generalise and treatment at different Strahler orders varies according to an *ad-hoc* scheme. On initialisation, the branching structure of their trees is selected randomly to follow morphological constraints, but from that point on, the tree topology is fixed. They use simulated annealing to optimise the orientations of the epicardial part of this structure subject to constraints, but not to optimise the topology. The major differences with the algorithm presented here are that (1) swap node updates are included that are able to explore the full configuration space of the topology of the tree, rather than setting up the tree structure on initialisation (2) all levels in the tree are treated with the same universal set of principles (3) experimental data is not required as an input to this algorithm, with the exception of the tissue shape, so any agreement with morphological data is a direct result of the algorithm and is not caused by the introduction of experimental morphological data into the algorithm.

Having recognised the advantages, it is also necessary to recognise current limitations to our algorithm. The algorithm currently only predicts the arrangement of arterial networks, and does not include venous drainage. It is not currently possible to include anastamoses in the method. These tend to be found near joints with significant movement to maintain constant downstream flow, with examples including the circle of Willis in the brain which counteracts neck movement and the dual supply of the cerebellum from PCA and basilar arteries. The possible combinations of vessels increases rapidly with the number of segments considered and this makes the computational requirements for optimising very large networks of vessels challenging (as the number of combinations increases factorially). This means that the smallest vessels represented in the trees are much larger than the end arterioles that contribute most to hydraulic resistance. As a consequence of this limitation we have had to make a number of approximations, such as running the model for one hemisphere and then symmetrising, whereas in practice there are asymmetries between regions of the cortex in left and right hemispheres.

The least good comparison is with vessel length. It is expected that smaller R_{ex} leads to small increases in vessel length at the highest Strahler order, because the vessels would have to follow the surface of the brain over a longer distance before penetrating the tissue. Ideally, trees would be grown using the physiological value of $R_{\text{ex}} = 50\mu$m. It is estimated that meaningful examination of trees with $R_{\text{ex}} = 50\mu$m would require trees with the order of 100000 segments, so that the smallest vessel radius is less than R_{ex}. This is outside our current computational capability, as discussed in the methods section. The simulated annealing algorithm is challenging to parallelise and there is no overall consensus on how to do this. Parallel SA may work well for some problems, but is generally far from perfectly parallel and at worst may offer the same performance as a single processor while using significantly more resource [19]. Nevertheless, there may be parallel simulated annealing algorithms suitable for this problem and this is suggested as a future extension. Alternative optimisation techniques, more suitable for distributed

computing, could also be considered for future extensions.

Overall, the algorithm and model presented here offer several advantages over existing techniques. The SALVO algorithm presented here is capable of approaching the global cost minimum, handling complex organ shapes and excluding large vessels from tissue. This is superior to previous techniques, which need to be adapted for each situation or require detailed experimental data to run, making application to new organs difficult. SALVO has been shown to be capable of growing detailed vascular trees for two large organs with complex vasculature (the heart and brain). The *in-silico* model presented here reproduces features that would be difficult, if not impossible, to reproduce with other available algorithms, without the need for detailed measurements of morphological data. Obtaining this level of detail over such a large structure would also be a major challenge for imaging techniques.

In summary we have introduced the SALVO algorithm for the cerebral arteries, and compared the resulting arterial trees against data derived from MRI scans. Further extensions should demonstrate the possibility of growing complementary arterial and venous vascular structures, focus on greater efficiency to allow the growth of much larger trees (including multiscale growth), and include the possibility of describing tortuous vessels.

Acknowledgements

JK acknowledges support from EPSRC grant EP/P505046/1. EC acknowledges support from EPSRC grant EP/L025884/1. The authors declare no competing interests. The authors would also like to thank Mark Horsfield (Xinapse systems) for help with the MRI scans.

Authors' contributions

JK developed the codes, acquired, analysed and interpreted data. EC managed MRI data and co-supervised the project. JPH conceived the study, developed initial versions of the algorithm, contributed to the codes, acquired, analysed and interpreted data, and supervised the project. All authors contributed to writing the article.

[1] S. J. Payne. *Cerebral Blood Flow and Metabolism: A Quantitative Approach.* Singapore: World Scientific,, 2017.

[2] Francis Cassot, Frederic Lauwers, Céline Fouard, Steffen Prohaska, and Valerie Lauwers-Cances. A novel three-dimensional computer-assisted method for a quantitative study of microvascular networks of the human cerebral cortex. *Microcirculation*, 13(1):1–18, January 2006.

[3] C.D. Murray. The Physiological Principle of Minimum Work: I. The Vascular System and the Cost of Blood Volume. *Proc. Natl. Acad. Sci.*, 12(3):207–14, March 1926.

[4] S Rossitti and J Löfgren. Vascular dimensions of the cerebral arteries follow the principle of minimum work. *Stroke*, 24(3):371–377, 1993.

[5] N.W. Witt et al. *Artery Research*, 4:75–80, 2010.

[6] W Schreiner and P F Buxbaum. Computer-optimization of vascular trees. *IEEE Trans. Biomed. Eng.*, 40(5):482–491, May 1993.

[7] B Kaimovitz et al. A full 3-D reconstruction of the entire porcine coronary vasculature. *Am. J. Physiol. Heart Circ. Physiol.*, 299(July 2010):1064–1067, 2010.

[8] J Keelan, E M L Chung, and J P Hague. Simulated annealing approach to vascular structure with application to the coronary arteries. *R. Soc. Open. Sci.*, 3:150431, 2016.

[9] Peiying Liu, Jinsoo Uh, Michael D. Devous, Bryon Adinoff, and Hanzhang Lu. Comparison of relative cerebral blood flow maps using pseudo-continuous arterial spin labeling and single photon emission computed tomography. *NMR Biomed.*, 25(5):779–786, 2012.

[10] Susan N. Wright, Peter Kochunov, Fernando Mut, Maurizio Bergamino, Kerry M. Brown, John C. Mazziotta, Arthur W. Toga, Juan R. Cebral, and Giorgio A. Ascoli. Digital reconstruction and morphometric analysis of human brain arterial vasculature from magnetic resonance angiography. *NeuroImage*, 82:170–181, 2013.

[11] http://cng.gmu.edu/brava.

[12] R. Fahraeus and T. Lindqvist. The viscosity of the blood in narrow capillary tubes. *Am. J. Physiol.*, 96:562–568, 1931.

[13] Geoffrey B West, James H Brown, and Brian J Enquist. A general model for the origin of allometric scaling laws in biology. *Science*, 276(5309):122–126, 1997.

[14] Y Liu and G S Kassab. Vascular metabolic dissipation in Murray's law. *Am. J. Physiol. Heart Circ. Physiol.*, 292(3):H1336–H1339, 2007.

[15] I.M.S. Wilkinson, J.W.D. Bull, G.H. du Boulay, J. Marshall, R.W.Ross Russell, and L. Symon. The heterogeneity of blood flow throughout the normal cerebral hemisphere. In M. Brock, C. Fieschi, D.H. Ingvar, N.A. Lassen, and K. Schürmann, editors, *Cerebral Blood Flow*, pages 17–18. Berlin: Springer,, 1969.

[16] AR Pries, Timothy W Secomb, P Gaehtgens, and JF Gross. Blood flow in microvascular networks. experiments and simulation. *Circ. Res.*, 67(4):826–834, 1990.

[17] Heinz Breu, Joseph Gil, David Kirkpatrick, and Michael Werman. Linear time euclidean distance transform algorithms. *IEEE Trans. Pattern Anal. Mach. Intell.*, 17(5):529–533, 1995.

[18] Emile Aarts, Jan Korst, and Wil Michiels. Simulated annealing. In E K Burke and G Kendall, editors, *Search methodologies*, pages 187–210. Berlin: Springer,, 2005.

[19] Z. Lou and J. Reinitz. *Parallel Comput.*, 53:23–31, 2016.

[20] Z. L. Jiang, G. S. Kassab, and Y. C. Fung. Diameter-defined Strahler system and connectivity matrix of the pulmonary arterial tree. *J. Appl. Physiol.*, 76(2):882–892, Feb 1994.

[21] S. Standring, editor. *Gray's anatomy*, chapter 19. Elsevier, 41 edition, 2016. (See Figs. 19.2 and 19.4).

[22] Persistence of Vision Pty. Ltd. (2019). Persistence of Vision Raytracer (Version 3.7) [Computer Software].

[23] A.A. Linninger, I.G. Gould, T Marrinan, C.Y. Hsu, M. Chojecki, and A. Alaraj. Cerebral microcirculation and oxygen tension in the human secondary cortex. *Ann. Biomed. Eng.*, 41:2264–2284, 2013.

[24] J P Hague, C Banahan, and E M L Chung. *Phys. Med. Biol.*, 58:4381–4394, 2013.

[25] C. Wang, J. B. Bassigthwaighte, and L. J. Weissman. Bifurcating distributive system using monte carlo method. *Math. Comput. Model.*, 16:91–98, 1992.

[26] Holger Perfahl, Helen M. Byrne, Tingan Chen, Veronica Estrella, Tomás Alarcón, Alexei Lapin, Robert A. Gatenby, Robert J. Gillies, Mark C. Lloyd, Philip K. Maini, Matthias Reuss, and Markus R. Owen. Multiscale modelling of vascular tumour growth in 3d: The roles of domain size and boundary conditions. *PLoS ONE*, 6(4):e14790, 04 2011.

[27] J.A. Nagy, S-H Chang, A.M.Dvorak, and H.F.Dvorak. Why are tumour blood vessels abnormal and why is it important to know? *British Journal of Cancer*, 100:865–869, 2009.

[28] R Karch, F Neumann, M Neumann, and W Schreiner. Staged growth of optimized arterial model trees. *Ann. Biomed. Eng.*, 28(5):495–511, May 2000.

[29] W Schreiner, F Neumann, M Neumann, R Karch, A End, and S M Roedler. Limited Bifurcation Asymmetry in Coronary Arterial Tree Models Generated by Constrained Constructive

Optimization. *J. Gen. Physiol.*, 109(2):129–140, 1997.

[30] Wolfgang Schreiner, Rudolf Karch, Martin Neumann, Friederike Neumann, Paul Szawlowski, and Susanne Roedler. Optimized arterial trees supplying hollow organs. *Med. Eng. Phys.*, 28(5):416–429, 2006.

[31] HorstK. Hahn, Manfred Georg, and Heinz-Otto Peitgen. Fractal aspects of three-dimensional vascular constructive optimization. In Gabriele A. Losa, Danilo Merlini, Theo F. Nonnenmacher, and Ewald R. Weibel, editors, *Fractals in Biology and Medicine*, Mathematics and Biosciences in Interaction, pages 55–66. Birkhäuser Basel, 2005.

Appendix: Modified diameter defined Strahler order scheme

The diameter defined Strahler order (DDSO) scheme from [20] uses radius information to improve the Strahler order scheme. The algorithm in [20] relies on the use of the standard deviation of the radii within individual Strahler orders, which is only strictly valid if the data are Gaussian distributed. In practice this is not guaranteed, and is in fact not expected since the iterative DDSO algorithm introduces a lower radius cutoff at each Strahler order, thus skewing the data.

A more general modified diameter defined Strahler order (MDDSO) scheme is proposed that can handle skewed data. For convenience, the 25th and 75th percentiles are used to define the bins, although any percentiles could be used (e.g. 15th and 85th, which approximately match the standard deviation if data are Gaussian). Then the algorithm is as follows:

(i) Calculate the Strahler order.

(ii) Determine 25th and 75th percentiles for radii in each order, $P_{25}^{(i)}$ and $P_{75}^{(i)}$ respectively, where i represents order.

(iii) Scanning from the end nodes of the tree, when two vessels meet, identify the vessel with largest order, O. This order increments in the parent vessel if and only if the radius is greater than $(P_{75}^{(O)} + P_{25}^{(O+1)})/2$

(iv) Repeat steps (ii)-(iv) until the mean radius at each order converges.

Examples of how results change with the modified scheme can be seen in Fig. 12. The changes are relatively minor, with the main difference a small reduction of the mean radius at each order. If 15th and 85th percentiles are used, and data are Gaussian, then the two schemes are expected to be identical.

Appendix: Download of model

Instructions for download of the Simulated Annealing Model of the Brain (SAMbrain) vasculature in SWC format can be found here: http://physics.open.ac.uk/∼jphague/SAMbrain/.

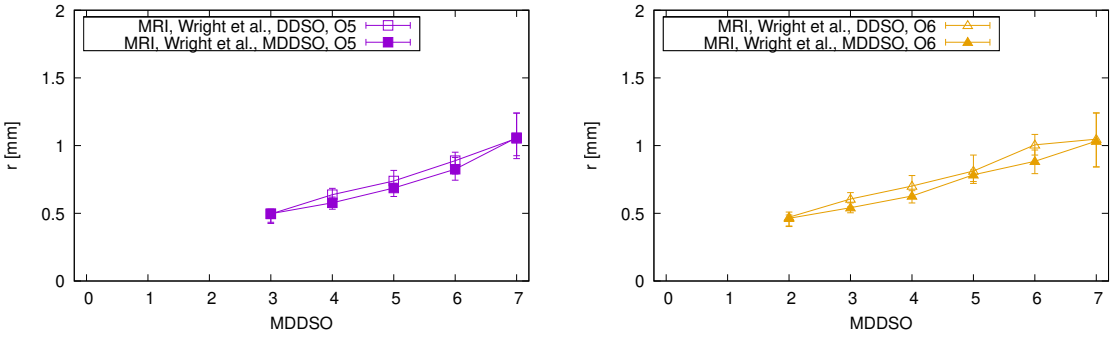

Figure 12. Comparisons of MDDSO with DDSO.